Geophysical Research Letters

RESEARCH LETTER
10.1029/2019GL083558

Dissolution Dominates Silica Cycling in a Shelf Sea Autumn Bloom

Alex J. Poulton[1,2], Kyle M.J. Mayers[3,4], Christopher J. Daniels[1], Mark C. Stinchcombe[1], E. Malcolm S. Woodward[5], Joanne Hopkins[6], Julianne U. Wihsgott[6], and Claire E. Widdicombe[5]

[1]National Oceanography Centre, Southampton, UK, [2]Now at The Lyell Centre for Earth and Marine Science and Technology, Heriot-Watt University, Edinburgh, UK, [3]Ocean and Earth Sciences, University of Southampton, Southampton, UK, [4]Now at NORCE Norwegian Research Centre, Bergen, Norway, [5]Plymouth Marine Laboratory, Plymouth, UK, [6]National Oceanography Centre, Liverpool, UK

Key Points:
- Rates of biogenic silica dissolution were greater than rates of production during late autumn
- A large fraction of detrital biogenic silica was present, with living biomass a minor fraction
- Low-light and high detrital biogenic silica promotes net dissolution rather than net production

Correspondence to:
A. J. Poulton,
a.poulton@hw.ac.uk

Citation:
Poulton, A. J., Mayers, K. M. J., Daniels, C. J., Stinchcombe, M. C., Woodward, E. M. S., Hopkins, J., et al (2019). Dissolution dominates silica cycling in a shelf sea autumn bloom. *Geophysical Research Letters*, *46*, 6765–6774. https://doi.org/10.1029/2019GL083558

Received 2 MAY 2019
Accepted 29 MAY 2019
Accepted article online 4 JUN 2019
Published online 24 JUN 2019

Abstract Autumn phytoplankton blooms represent key periods of production in temperate and high-latitude seas. Biogenic silica ($bSiO_2$) production, dissolution, and standing stocks were determined in the Celtic Sea (United Kingdom) during November 2014. Dissolution rates were in excess of $bSiO_2$ production, indicating a net loss of $bSiO_2$. Estimated diatom $bSiO_2$ contributed ≤10% to total $bSiO_2$, with detrital $bSiO_2$ supporting rapid Si cycling. Based on the average biomass-specific dissolution rate (0.2 day^{-1}), 3 weeks would be needed to dissolve 99% of the $bSiO_2$ present. Negative net $bSiO_2$ production was associated with low-light conditions (<4 $E{\cdot}m^{-2}{\cdot}day^{-1}$). Our observations imply that dissolution dominates Si cycling during autumn, with low-light conditions also likely to influence Si cycling during winter and early spring.

Plain Language Summary Small marine microalgae called diatoms are responsible for significant levels of primary production in support of marine ecosystems. Diatom cells are formed from silica dissolved in seawater; however, diatom cells may also readily dissolve in seawater. Observationsof silica uptake and dissolution during the autumn period of enhanced microalgal productivity in a shelf seafound a nonliving detrital pool of diatomaceous material, which was dissolving faster than the few diatomspresent were making new cells. These observations highlight that certain periods of the year may be associated with rapid rates of dissolution and hence are important for recycling of material prior to the winter period when nutrient budgets in the water-column are set for the following year.

1. Introduction

Despite representing <10% of the ocean, shelf seas represent ~30% of primary production (~15 Pg C/year, Field et al., 1998). Annually, spring blooms, triggered by stratification and optimal growth conditions (Lindeman & St. John, 2014; Taylor & Ferrari, 2011), dominate production, with weaker rates during the stratified summer terminated by increased autumn mixing (Findlay et al., 2006; Painter et al., 2016; Perry et al., 2008; Wihsgott et al., 2018). During summer, phytoplankton adapt to low nutrient conditions in surface waters and low light at the base of the surface mixed layer (SML), forming a subsurface chlorophyll maximum (SCM; Hickman et al., 2009). Weakening stratification is associated with a secondary biomass peak, considered an "autumn bloom," which may reflect elevated production and/or redistribution of SCM material (Findlay et al., 2006; Painter et al., 2016; Perry et al., 2008).

Diatoms represent ~44% of marine production, sustain ecosystems, and contribute to deep-sea export (Nelson et al., 1995; Tréguer et al., 2018; Tréguer & De La Rocha, 2013). Diatoms dominate the global Si budget, producing 240 Tmol Si/year of biogenic silica ($bSiO_2$) (Tréguer & De La Rocha, 2013), or ~22 Pg C/year based on a 7.6-mol/mol carbon (C) to Si ratio (Brzezinski, 1985; Nelson et al., 1995). Coastal waters are key for $bSiO_2$ production (Tréguer & De La Rocha, 2013), with ~60% of global $bSiO_2$ production (equivalent to ~13 Pg C/year or 90% of coastal production) occurring in shelf and upwelling environments. Diatoms possess several traits supporting their ecological success: a protective silicified cell wall (Hamm et al., 2003) and high intrinsic growth rates allowing them to proliferate with high nutrients and low grazing (Tréguer et al., 2018). Silicic acid ($Si(OH)_4$) requirements further define diatom biogeography, especially for species with high or low cellular $bSiO_2$ (Fragoso et al., 2018; Tréguer et al., 2018).

Despite the success of diatoms, the ocean is undersaturated with $Si(OH)_4$, and the corrosive basic nature of seawater pH (Martin-Jezequel et al., 2000) leads to $bSiO_2$ dissolution if unprotected by the organic components of the cell wall (Bidle & Azam, 1999; Van Cappellen et al., 2002). Dissolution of $bSiO_2$ is controlled by the following: temperature, grazing, bacterial activity, and frustule chemistry (Bidle et al., 2003; Bidle & Azam, 1999, 2001; Dugdale & Wilkerson, 1998; Natori et al., 2006; Nelson et al., 1995).

The global Si cycle is dominated by extensive Si recycling (low riverine influxes, minimal burial; Tréguer et al., 1995; Tréguer & De La Rocha, 2013), with $bSiO_2$ dissolution a critical mechanism resupplying Si (Nelson et al., 1995, 1996). Ratios of $bSiO_2$ dissolution (D) to production (P) range from 0.05–5.8, with the upper-ocean average 0.5–0.6 (Nelson et al., 1995; Tréguer & De La Rocha, 2013). Low D:P ratios (<0.1) are typical of diatom blooms, with D:P ratios >0.5 indicating that the majority of $bSiO_2$ produced is recycled within the upper ocean (Brzezinski et al., 2003; Tréguer & De La Rocha, 2013).

Ratios of D:P represent the fraction of $bSiO_2$ production supported by upper-ocean Si-recycling, or expressed as 1-D:P, the fraction of $bSiO_2$ production supported by "new" Si from the deep sea (Brzezinski et al., 2003). Most studies measuring rates of production and dissolution have occurred during spring and summer, with coastal studies almost exclusively from upwelling sites (Krause et al., 2010; Tréguer & De La Rocha, 2013). Despite the importance of Si dissolution in controlling upper-ocean Si dynamics, and the fate of diatom carbon, uncertainty remains of what controls the variability in D:P ratios, or how this impacts the Si cycle (Beucher et al., 2004, 2004; Tréguer & De La Rocha, 2013).

With this in mind, this study examined $bSiO_2$ production and dissolution, alongside measurements of $bSiO_2$ pool composition and size, during an autumn shelf sea bloom. The specific objectives were to (1) measure the magnitude of $bSiO_2$ production and examine the composition of the diatom community; (2) examine rates of $bSiO_2$ dissolution when the water column is "resetting" before winter; and (3) compare ratios of dissolution to production (D:P) and the factors driving them in order to provide information on Si recycling.

2. Materials and Methods

2.1. Sampling

Sampling occurred in the Celtic Sea on board the RRS *Discovery* (cruise DY018, 9 November to 2 December 2014) at two sites; the Central Celtic Sea (CCS; 49°24′N, 8°36′W; 145-m water depth; $n = 4$), and the Shelf Break (CS2; 48°34.26′N, 9°30.58′W; 203 m; $n = 2$) (Figure 1a). The Celtic Sea was selected as a study site to examine Si cycling due to its long residence time, minimal coastal influence, and isolation from fronts or topographic features (see Ruiz-Castillo et al., 2018). A mooring was deployed at CCS (sited at 49°23′N, 8°35′W) for 17 months (26 March 2014 to 25 July 2015), collecting water column structure, chlorophyll-*a* fluorescence, and meteorological data (Figure 1; see also Wihsgott et al., 2016, 2018, 2019).

During the cruise, water samples were collected from six light depths (60%, 40%, 20%, 10%, 5%, and 1% of surface irradiance) in 20-L Niskin bottles (OTE: Ocean Test Equipment) on a CTD rosette sampler deployed predawn (0200–0600 local time). Depths were determined by back calculation of the vertical attenuation coefficient (K_d, m^{-1}) of photosynthetically active radiation (PAR), with the base of the SML at or close to the depth of the euphotic zone (1% surface irradiance) (Poulton et al., 2018).

Depth of the SML was determined from density profiles, from the ships CTD and mooring time-series, by identifying where potential density increased by 0.02 kg m^{-3} above the 10-m value (Poulton et al., 2018; Wihsgott et al., 2019). A 2π PAR irradiance sensor (Skye Instruments, SKE 510) on the RRS *Discovery* and a quantum PAR meter (LiCor Inc., USA) on the mooring-measured incident irradiance (E_0). Average SML irradiance ($\bar{E}_{SML}$) was determined following Poulton et al. (2018). Mooring fluorescence data were determined by a Seapoint fluorometer, standardized using fluorescent sulfate microspheres (FluoSpheres, ThermoFisher Scientific) with nighttime data only to avoid daytime quenching (Wihsgott et al., 2018, 2019).

2.2. Silica Cycling

Micromolar (μmol/kg) concentrations of nitrate + nitrite (NO*x*) and silicic acid ($Si(OH)_4$) were measured with a Bran and Luebbe segmented flow colorimetric autoanalyzer following Woodward and Rees (2001). Samples were taken in acid-cleaned, aged, HDPE bottles, and clean sample handing procedures followed. All samples were analyzed within 1–2 hr of collection. Certified reference materials were used daily

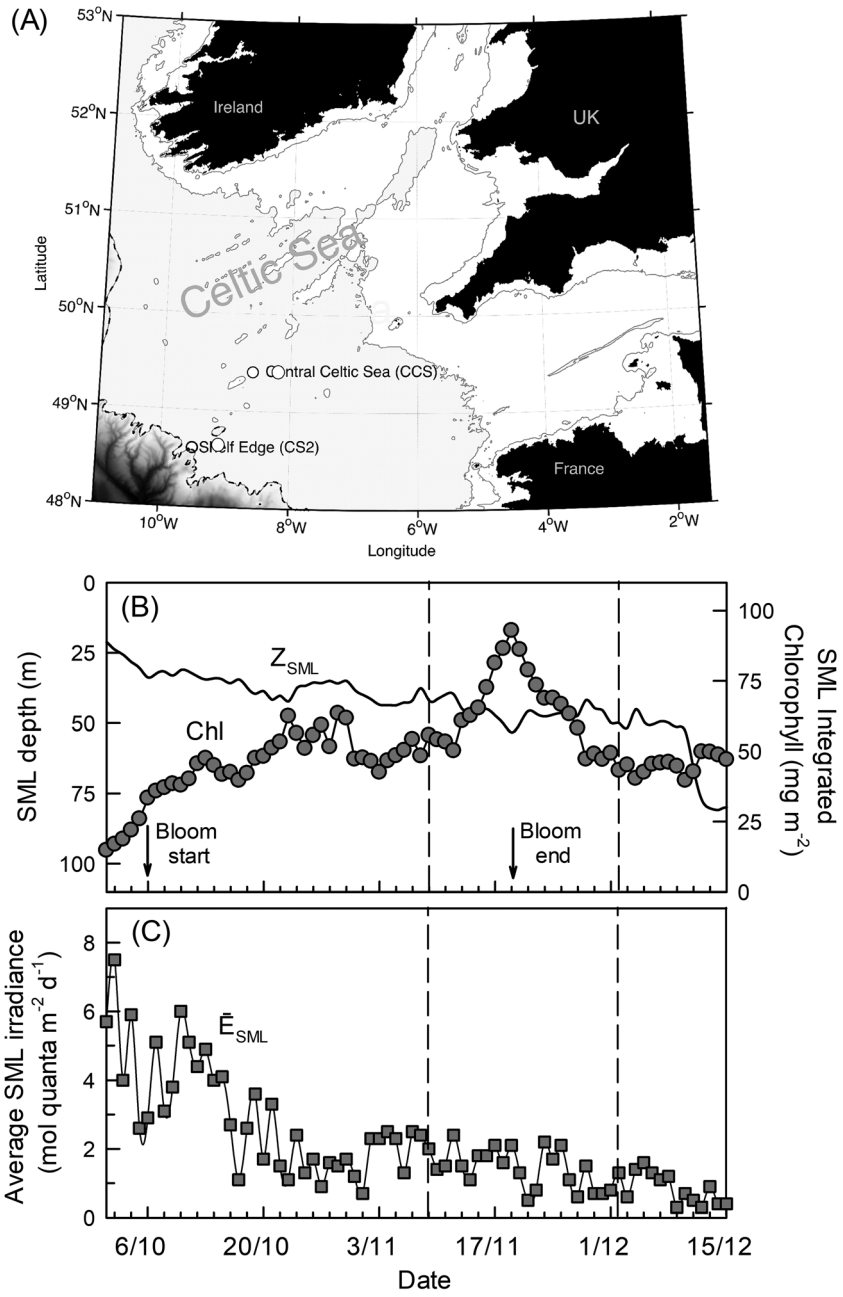

Figure 1. Map of sampling sites, Central Celtic Sea (CCS) mooring, and time series of surface mixed layer (SML) properties. (a) Map of sampling and mooring sites CCS and Shelf Edge (CS2), (b) mooring-derived time series of SML depth (Z_{SML}, m) and SML integrated chlorophyll (Chl, mg m^{-2}), and (c) average SML irradiance ($\bar{E}_{SML}$, E·m^{-2}·day^{-1}). Dashed lines on (b) and (c) indicate cruise period (9 November 2014 to 2 December 2014) and arrows indicate start date (6 October 2014) and end date (20 November 2014) of the autumn bloom at CCS as defined by Wihsgott et al. (2018).

(KANSO, Japan), and analytical procedures followed International GO-SHIP recommendations (Hydes et al., 2010). The typical uncertainty of the analytical results were between 2% and 3%, and the limits of detection for nitrate and phosphate were 0.02 μmol L^{-1}, while $Si(OH)_4$ was always higher than the detection limits. Measurements of particulate silica concentrations ($bSiO_2$; μmol Si kg^{-1}) were made on 0.5-L samples filtered onto 0.8-μm polycarbonate filters, digested in 0.2 M·NaOH at 85 °C for 1 hr and neutralized with 0.2 M·HCl (Ragueneau & Tréguer, 1994). Sample analysis was with a SEAL QuAAtro autoanalyzer (Poulton et al., 2006) using standard techniques.

Daily measurements of gross $bSiO_2$ production (ρ_P) and net $bSiO_2$ production (ρ_N) were made at the six depths, and followed Krause et al. (2010) (see also Poulton et al., 2006). Duplicate water samples were spiked with 0.03-μCi high specific activity (2.06 μCi/mL) ^{32}Si-labeled Si $(OH)_4$ and incubated for 24 hr in 70-mL polycarbonate bottles (Corning™). Incubations were filtered onto 25-mm 0.8-μm polycarbonate (Whatman Nucleopore™) filters under gentle vacuum. Filters were digested with 0.2-M NaOH in 20-mL plastic scintillation vials (PerkinElmer UK), at 85 °C for 1 hr. After cooling, 0.2-M HCl was added and 15 mL of UltimaGold™ liquid scintillation cocktail. Activity on the filters was determined on a 1220 Quantulus™ ultralow level liquid scintillation counter (Wallac, Finland) after >100 days, allowing secular equilibrium.

Daily ρ_P and biomass-normalized specific uptake (V_P) were calculated after Krause et al. (2010). Triplicate unspiked samples, collected alongside samples for ρ_P determination were incubated in parallel for 24 hr, with differences between initial and end $bSiO_2$ concentrations considered as net $bSiO_2$ production (ρ_N), with dissolution defined by the difference between ρ_P and ρ_N (Krause et al., 2010). Biomass-normalized specific dissolution (V_D) was calculated after Krause et al. (2010).

Incubations under different daily light doses followed Poulton et al. (2018) in a modified refrigeration container, with temperatures ±1–2 °C of those in situ. Irradiance was provided by one to three daylight simulated LED panels (Powerpax, UK), combined with neutral density filters (Lee Filters™, UK), to achieve target irradiance for each light level (sampling depth). These were 5.4 E·m^{-2}·day^{-1} (60% incident irradiance light depth), 4.8 E·m^{-2}·day^{-1} (40%), 2.3 E·m^{-2}·day^{-1} (20%), 0.8 E·m^{-2}·day^{-1} (10%), 0.5 E·m^{-2}·day^{-1} (5%), and 0.2 E·m^{-2}·day^{-1} (1%). Daily light doses reflected the November seasonal and depth-specific irradiance, based on analysis of 10 years of MODIS Aqua data (see Poulton et al., 2018, for further details). Cruise average daily integral E_0 was a good match (9.6 E·m^{-2}·day^{-1}, range 7.7–12.1 E·m^{-2}·day^{-1}) to that from long-term satellite data (average E_0 for CCS (2003–2013), 9.4 E·m^{-2}·day^{-1}).

2.3. Chlorophyll-*a*, Primary Production and Diatom Biomass

Chlorophyll-*a* (Chl) concentrations (mg m^{-3}) were measured on 0.2-L water samples filtered onto 25-mm Whatman GF/F filters, and extracted in 6-mL 90% acetone (Sigma-Aldrich, UK) at 4 °C for 18–24 hr. Chl fluorescence was measured on a Turner Designs Trilogy™ fluorometer using a nonacidification module calibrated with solid and pure Chl standards (Sigma-Aldrich, UK). Daily net primary production (NPP) rates were determined following Poulton et al. (2018). Four samples in 70-mL polycarbonate bottles from each depth were spiked with 1,258–1,628 kBq of ^{14}C-labeled sodium bicarbonate (PerkinElmer, UK), with 1-mL of borate-buffered formaldehyde (~2% final solution) added to one bottle as a formalin-killed blank. Samples were incubated in parallel to ρ_P and terminated by filtering onto 25-mm 0.45-μm Whatman Nucleopore™ polycarbonate filters, with extensive rinsing to remove unfixed isotope. Organic (NPP) carbon fixation was determined using the microdiffusion technique (as in Poulton et al., 2018) with 1-mL of 1% orthophosphoric acid added to remove ^{14}C-particulate inorganic carbon and 10-mL of UltimaGold™ (PerkinElmer, UK) liquid scintillation cocktail. Filter activity was determined on-board a Tri-Carb 3100TR (Perkin-Elmer) liquid scintillation counter.

Diatom cell counts were analyzed from each sampling depth by light microscopy of samples in 250-mL brown glass bottles, preserved in acidic Lugol's solution (2% final solution), and analyzed with a Leica DMI4000B inverted microscope (Widdicombe et al., 2010). Diatom $bSiO_2$ was estimated by applying the average cell Si content (8.14 pmol Si cell^{-1}) from Brzezinski (1985) to the diatom cell counts.

3. Results

3.1. Celtic Sea Hydrography

At CCS, ocean cooling commenced in early October, steadily deepening the SML until the end of December, primarily by wind-induced mixing (Figure 1b; Wihsgott et al., 2019). Integrated Chl (Figure 1b) increased parallel to SML deepening, up until 12 November, when there was an increase to 93 mg m^{-2}, followed by a decline and little variation until the end of December. Average SML irradiance ($\bar{E}_{SML}$) calculated from the CCS mooring data declined rapidly from 6 E·m^{-2}·day^{-1} to <4 E·m^{-2}·dat^{-1} from 24 October

Table 1
Hydrography and Euphotic Zone Integrals for Si Stocks and Si Cycling for Celtic Sea Sampling Sites in November 2014

	Site							
	CCS	CCS	CS2	CS2	CCS	CCS		
	Date							
Variables	10 Nov	12 Nov	18 Nov	20 Nov	22 Nov	25 Nov	Mean	Units
SML depth	44	32	58	58	54	52	50	(m)
SML temperature	13.7	13.6	13.9	14.1	13.1	12.8	13.5	(°C)
Surface NO*x*	2.1	2.1	3.5	2.6	1.8	2.5	2.4	(μmol N L^{-1})
Surface Si $(OH)_4$	0.9	0.8	1.4	1.3	1.1	1.1	1.1	(μmol Si L^{-1})
Incidental irradiance	8.4	11.9	7.7	9.3	8.1	12.1	9.6	(E·m^{-2}·day^{-1})
SML average irradiance	1.6	2.3	1.8	1.9	1.4	2.5	1.9	(E·m^{-2}·day^{-1})
Chlorophyll *a*	59.7	37.4	54.4	57.6	68.7	70.8	58.1	(mg Chl m^{-2})
Net primary production	37.0	18.5	22.5	26.3	42.9	46.9	31.3	(mmol·C·m^{-2}·day^{-1})
Euphotic Si $(OH)_4$	37.1	24.4	90.6	69.2	45.1	52.2	53.1	(mmol Si m^{-2})
Total $bSiO_2$	ND	9.3	15.6	12.1	9.2	11.6	11.6	(mmol Si m^{-2})
Diatom $bSiO_2$	1.8	0.9	3.0	1.0	0.6	0.6	1.3	(mmol Si m^{-2})
Gross $bSiO_2$ production (ρ_P)	ND	0.5 (0.1)	2.2 (0.3)	1.4 (0.1)	0.3 (0.0)	0.7 (0.1)	1.0	(mmol·Si·m^{-2}·day^{-1})
Net $bSiO_2$ production (ρ_N)	ND	−2.6 (0.4)	0.4 (0.1)	−2.2 (0.1)	−1.4 (0.2)	−0.6 (0.1)	−1.3	(mmol·Si·m^{-2}·day^{-1})
Dissolution rate (*D*)	ND	3.1 (0.6)	1.8 (0.3)	3.6 (0.2)	1.6 (0.3)	1.3 (0.3)	2.3	(mmol·Si·m^{-2}·day^{-1})
bSiO2-specific dissolution rate (V_D)	ND	0.3	0.1	0.3	0.2	0.1	0.2	(day^{-1})
Ratio of dissolution (*D*) to production (*P*)	ND	6.2	0.8	2.6	5.3	1.9	3.4	

Note. ND indicates not determined. Values in parenthesis for $bSiO_2$ production and dissolution indicate standard errors.

(Figure 1c). $\bar{E}_{SML}$ then declined slowly until mid-December, with values <3 E·m^{-2}·day^{-1} from 24 October, and <2 E·m^{-2}·day^{-1} from 25 November.

Ship measurements showed similar trends to the mooring data (Table 1; Figures 1b and 1c). Deeper SML occurred at CS2 than CCS, with SML temperatures warmer (~0.5 °C) at CS2 than CCS. Chl integrals from the cruise (Table 1) were similar in magnitude to the mooring data, due to similarity in SML and euphotic zone depths (Poulton et al., 2018). Chl ranged from 37–71 mg m^{-2}, with lower integrals at CS2 than CCS, and an increase of 10–30 mg m^{-2} between early and late November (Table 1). Incidental irradiance varied from 7.7–12.1 E·m^{-2}·day^{-1} over November (average 9.6 E m^{-2} day^{-1}; Table 1). Little difference between CS2 and CCS was seen in terms of $\bar{E}_{SML}$, with an average of 1.9 E·m^{-2}·day^{-1} (20% of E_0; Table 1), broadly similar to the mooring data (Figure 1b).

Surface nutrient concentrations (NO*x*, Si $(OH)_4$) showed variability between CS2 and CCS, with concentrations slightly higher at CS2 than CCS (Table 1). Ratios of Si $(OH)_4$:NO*x* (mol/mol) ranged from 0.4–0.6, indicating shelf waters were depleted in Si $(OH)_4$ relative to NO*x*, with no obvious difference between CS2 and CCS. Integrated NPP showed a similar pattern to Chl with values ranging from 18.5–46.9 mmol C·m^{-2}·day^{-1} at CCS and from 22.5–26.4 mmol C·m^{-2}·day^{-1} at CS2 (Table 1).

3.2. Silica Stocks and Rates

Vertical SML profiles of Si $(OH)_4$ were uniform, apart from at CCS on 12 November when concentrations increased at the base of the SML (Figure 2a). In contrast, SML $bSiO_2$ was variable, though concentrations were 5–7 times lower than those of Si $(OH)_4$, ranging from 100–300 nmol Si L^{-1} (Figure 2b). Integrated Si $(OH)_4$ and $bSiO_2$ ranged from 24.4–90.6 mmol Si m^{-2} and 9.2–15.6 mmol Si m^{-2}, respectively (Table 1).

Diatom cell counts ranged from 1.2–12.8 cells ml^{-1}, with up to 22 taxa present. Numerically dominant diatoms included *Pseudo-nitzschia*, *Dactyliosolen* and *Chaetoceros*, whereas *Rhizosolenia*, *Dactyliosolen*, and *Guinardia* dominated carbon biomass (Widdicombe and Poulton, pers. obs.). No freshwater or estuarine-associated diatom taxa were identified. Diatom-specific $bSiO_2$ estimates were 10 times lower than total $bSiO_2$ and showed no consistent profile (Figure 2c). Apart from CS2 on 18 November, which had diatom-specific $bSiO_2$ concentrations of 30–60 nmol Si/L, all other sampling stations had diatom-specific $bSiO_2$ <

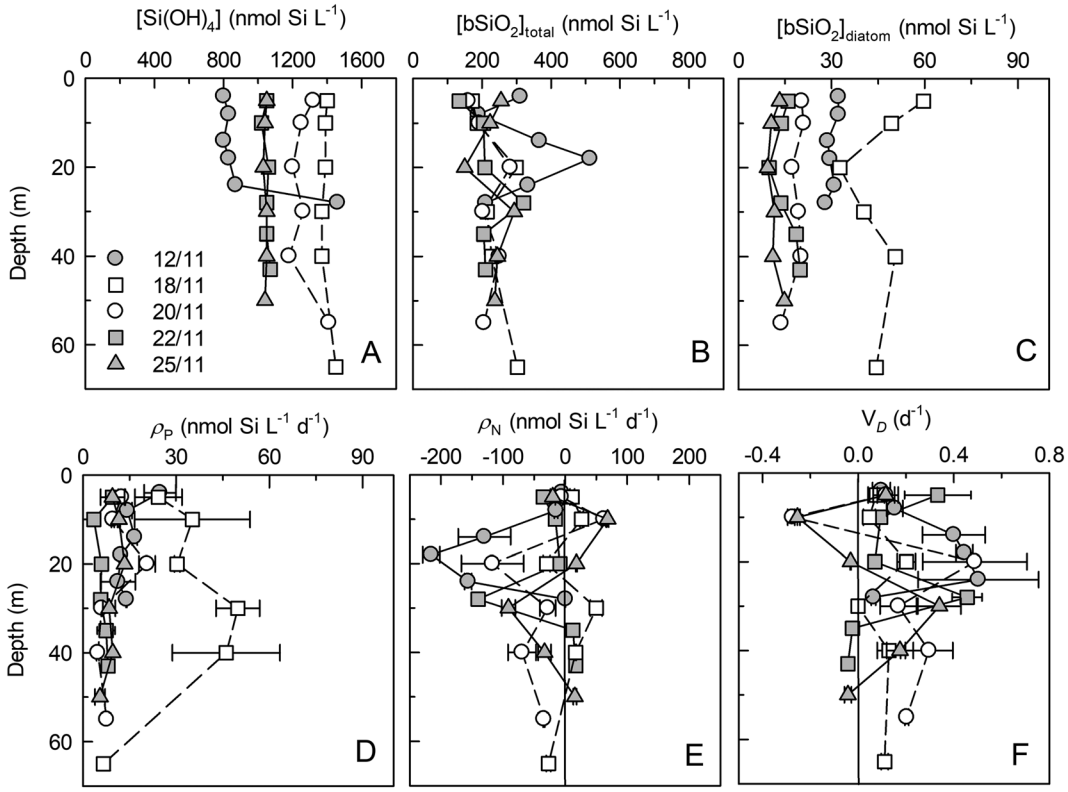

Figure 2. Vertical profiles of Si pool concentrations (nmol Si L^{-1}) and $bSiO_2$ dynamics. (a) silicic acid concentrations ($Si(OH)_4$), (b) total $bSiO_2$ concentration ($bSiO_{2total}$), (c) diatom $bSiO_2$ concentration ($bSiO_{2diatom}$), (d) gross $bSiO_2$ production (ρ_P, nmol $Si{\cdot}L^{-1}{\cdot}day^{-1}$), (e) net $bSiO_2$ production (ρ_N, nmol $Si{\cdot}L^{-1}{\cdot}day^{-1}$), and (f) biomass-specific dissolution rate (V_D, day^{-1}). Diatom $bSiO_2$ was estimated by applying the average cell Si content from Brzezinski (1985) to the diatom cell counts. Different sampling dates and locations are given as symbols (see Table 1 for dates and locations). Error bars are from triplicate measurements for each sampling depth.

30 nmol Si/L. Integrated diatom-specific $bSiO_2$ ranged from 0.6–3.0 mmol Si m^{-2} (Table 1). Ratios of diatom-specific $bSiO_2$ relative to total $bSiO_2$ ranged from 0.05–0.19 (average 0.10), indicating that ~10% of total $bSiO_2$ was associated with living diatom cells, suggesting a significant detrital fraction.

Vertical ρ_P profiles were uniform across the SML and for most stations were <20 nmol $Si{\cdot}L^{-1}{\cdot}day^{-1}$ (Figure 2d). Rates of ρ_P were higher at CS2 on 18 November (range 25–50 nmol $Si{\cdot}L^{-1}{\cdot}day^{-1}$) in association with high $bSiO_2$ concentrations (Figures 2b and 2d). Euphotic zone integrated ρ_P ranged from 0.28–2.14 mmol $Si{\cdot}m^{-2}{\cdot}day^{-1}$, with an average of 0.78 mmol $Si{\cdot}m^{-2}{\cdot}day^{-1}$ and no differences between sites or time (Table 1). The ratio of NPP to ρ_P (mol C: mol Si) for integrals, ranged from 11–153 with an average of 69, 9 times higher than the average diatom cellular ratio of C:Si (7.6, Brzezinski, 1985), and implies a low diatom contribution to NPP

Rates of ρ_N were either slightly positive or strongly negative across the water column (Figure 2e), with ρ_N ranging from 68 to −215 nmol $L^{-1}{\cdot}day^{-1}$ and an average of −29 nmol $L^{-1}{\cdot}day^{-1}$. Negative ρ_N implies net dissolution rather than net production (positive ρ_N), with inferred ρ_D rates well above ρ_P. Rates of ρ_D normalized to total $bSiO_2$ ranged from −0.3 to 0.5 day^{-1} (Figure 2f), with an average of 0.2 day^{-1} (Table 1). Integrated ρ_D rates were generally in excess of ρ_P for most sampling sites (Table 1), apart from CS2 on 18 November. High V_D reflects the strongly negative ρ_N and high $bSiO_2$ concentrations observed at all sampling sites. Ratios of *D*:*P* was strongly negative for all sampling sites (apart from CS2 on 18 November; Table 1), indicating that Si production could be fully supported by recycled $Si(OH)_4$.

4. Discussion

High NPP and Chl (Table 1 and Figure 1b; Poulton et al., 2018), prior to the wintertime breakdown of stratification, are indicative of the autumn bloom (Wihsgott et al., 2019). Based on SML and critical depth

(where growth equals losses), Wihsgott et al. (2019) determined that the autumn bloom started on 6 October (see Figure 1b), terminating 50 days later (20 November) when the SML deepened below the critical depth. Our observations characterize elevated carbon fixation and biomass during the late stages of this period.

Though the shelf edge (CS2) showed similar Chl and NPP to CCS, on 18 November it exhibited higher nutrient levels, $bSiO_2$ and Si-uptake, positive net $bSiO_2$ production, with a *D*:*P* ratio (0.8) indicative of "new" Si supporting 20% of $bSiO_2$ production. The Celtic Sea has an energetic internal wave field (Green et al., 2008; Vlasenko et al., 2014), with breaking waves at the shelf edge enhancing nutrient supplies (Sharples et al., 2009). During November 2014, stratification supported an internal tide (Wihsgott, 2018), with warm water at the shelf break from internal tidal mixing redistributing heat vertically (see Figure 2 in Ruiz-Castillo et al., 2018). Our observations indicate that this autumn diapycnal nutrient transfer supports $bSiO_2$ production; however, the limited nature of our observations means that the remainder of this paper will only consider the Si dynamics at CCS.

In contrast to NPP, integrated $bSiO_2$ production rates at CCS (Table 1) were similar to rates observed in the low-latitude Atlantic (<1 mmol·Si·m^{-2}·day^{-1}, Poulton et al., 2006, Krause et al., 2010) rather than diatom blooms in, for example, the subpolar Atlantic (6–167 mmol·Si·m^{-2}·day^{-1}, Brown et al., 2003), or Monterey Bay (5–108 mmol·Si·m^{-2}·day^{-1}, Brzezinski et al., 2003). High NPP and low $bSiO_2$ production, with C:Si ratios 9 times higher than diatom cells, imply that diatoms had limited impact in autumn. Diatom-specific NPP estimates (see Poulton et al., 2006), indicate that diatoms contributed an average of 12% to NPP. Unlike $bSiO_2$ production, standing stocks of $bSiO_2$ (Table 1) were relatively moderate, higher than the low-latitude Atlantic (<1 mmol Si m^{-2}, Poulton et al., 2006; 2.2–19.8 mmol Si m^{-2}, Krause et al., 2010), but lower than the subpolar Atlantic (10–148 mmol Si m^{-2}, Brown et al., 2003), or Monterey Bay (16–175 mmol Si m^{-2}, Brzezinski et al., 2003). Thus, the late autumn bloom at CCS was characterized by low $bSiO_2$ production, low diatom NPP contributions, but comparatively moderate levels of $bSiO_2$.

However, consideration of only ρ_P (gross production) fails to recognize the significant rates of $bSiO_2$ dissolution. Rates of $bSiO_2$ dissolution (Table 1) are similar to other studies, for example, in the Sargasso Sea (0.1–1.3 mmol Si m^{-2} day^{-1}, Krause et al., 2010) and Monterey Bay (0.6–6.5 mmol Si m^{-2} day^{-1}, Brzezinski et al., 2003). In these cases, however, $bSiO_2$ production was higher than $bSiO_2$ dissolution so that net production was positive (Brzezinski et al., 2003; Krause et al., 2010). At CCS in autumn, dissolution rates were higher than ρ_P, so *D*:*P* ratios were >1 (Table 1), and ρ_N (net production) was negative (Figure 2e). In effect, new $bSiO_2$ material was produced as fast as it was dissolved, although the two pools were not necessarily the same. The level of detrital $bSiO_2$ not associated with diatoms cells was estimated to be high at CCS (>90%), and rapid dissolution of dead diatoms has also been observed in the Bay of Brest and Southern Ocean (Beucher, Treguer, Corvaisier, Hapette, & Elskens, 2004; Beucher, Treguer, Corvaisier, Hapette, Pichon, & Metzl, 2004).

Ratios of $D{:}P > 1$, indicative of dissolution rates exceeding production rates, are thought to be possible only over short timescales or in limited localities (Tréguer & De La Rocha, 2013). High ratios have been observed in the Bay of Brest and Southern Ocean, and like the Celtic Sea, these are linked to high proportions of detrital $bSiO_2$ from grazing and cell death following blooms (Beucher, Treguer, Corvaisier, Hapette, & Elskens, 2004; Beucher, Treguer, Corvaisier, Hapette, Pichon, & Metzl, 2004). Applying the average biomass-specific dissolution rate (V_D ~0.2 day^{-1}; Table 1) implies an exponential decline in $bSiO_2$ that would take 22 days to reduce $bSiO_2$ levels to <1% of initial levels. If these biomass-specific dissolution rates continued during winter, this would support the upper-ocean dissolution of the autumn $bSiO_2$ pool prior to the spring bloom.

The source of the autumn $bSiO_2$ detrital pool also needs to be considered. Due to limited coastal influence at CCS (see Ruiz-Castillo et al., 2018) and an absence of estuarine diatoms, a terrestrial source for the material is unlikely. The depth (145 m) and persistent thermocline would also limit any potential sedimentary $bSiO_2$. In fact, the $bSiO_2$ pool represents only 3% of the estimated total water column inventory of Si (406 mmol Si m^{-2}, based on a 145-m water column and winter Si $(OH)_4$ ~2.8 μM, see Hydes et al., 2001), or 20% of the SML inventory of Si (55 mmol Si m^{-2}; Table 1). The total autumn $bSiO_2$ pool is also equivalent to only 10% of estimated Celtic Sea spring bloom $bSiO_2$ production (115 mmol Si m^{-2}), based on the Si $(OH)_4$ decline from winter (2.8 μM) to summer (0.5 μM; see Hydes et al., 2001). Taking the average diatom cell Si content from Brzezinski (1985) (8.14 pmol Si $cell^{-1}$), the total autumn $bSiO_2$ pool is roughly equivalent to only 30 cells

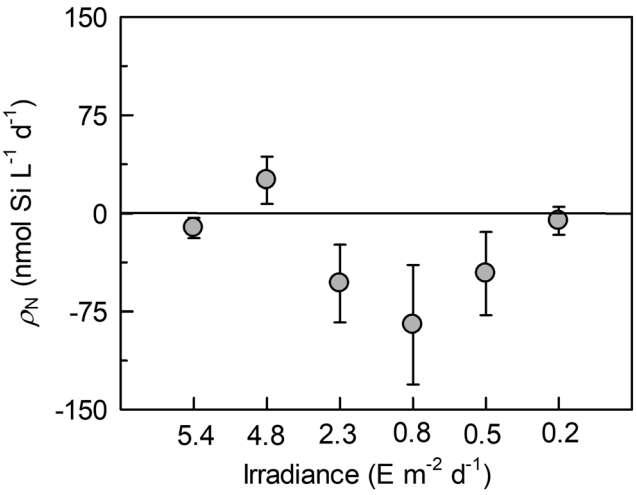

Figure 3. Possible irradiance controls on net $bSiO_2$ production (ρ_N, nmol $Si{\cdot}L^{-1}{\cdot}day^{-1}$) in terms of incubation irradiance ($E{\cdot}m^{-2}{\cdot}day^{-1}$). Values of ρ_N represent averages and standard errors ($n = 5$). Dashed line indicates ρ_N values of zero.

ml^{-1}. Though the detrital $bSiO_2$ is important for autumn Si cycling, contextually it is a small proportion of the total Si pool (re)cycled annually.

Diatoms are common features of shelf sea SCM (Barnett et al., 2019; Hickman et al., 2009). The summertime SCM at CCS contained 2.1 mg Chl m^{-3}, whilE the SML had 0.3 mg Chl m^{-3} (Wihsgott et al., 2019). When stratification broke down in early October (Figure 1b), nutrients and Chl were redistributed across the SML, with SML Chl increasing to 2.2 mg Chl m^{-3}, indicating that resupply of replenished nutrients by SML deepening was the driver of the autumn bloom (Wihsgott et al., 2019). Diatoms and $bSiO_2$ from the SCM may have been redistributed into the SML in early October, with (net) $bSiO_2$ production of only 0.3 mmol $Si{\cdot}m^{-2}{\cdot}day^{-1}$ (30% of measured production rates) needed to acquire the November $bSiO_2$ pool. Hence, November $bSiO_2$ is actually not high and low contribution to the total Si inventories, high detrital composition, and rapid dissolution rates imply that during the late autumn bloom diatom Si dynamics are limited by factors other than nutrient availability.

Light-limitation of the Celtic Sea autumn bloom has been described in terms of low growth rates (Poulton et al., 2018), and interactions between the SML and critical depth (Wihsgott et al., 2019). In the context of Si dynamics, vertical ρ_N profiles show little pattern, with both positive and negative ρ_N relative to depth (Figure 2e). If ρ_N are averaged for each incubation light-dose (Figure 3), then a vertical pattern is observed, with less negative ρ_N at higher irradiance levels (>4.8 $E{\cdot}m^{-2}{\cdot}day^{-1}$) and negative ones at lower levels (<2.3 $E{\cdot}m^{-2}{\cdot}day^{-1}$). This implies positive (net) $bSiO_2$ production at irradiance levels >4 $E{\cdot}m^{-2}{\cdot}day^{-1}$, higher than the compensation irradiances of Wihsgott et al. (2019) for net growth (1.2 and 3.0 $E{\cdot}m^{-2}{\cdot}day^{-1}$), or the $\bar{E}_{SML}$ for late October to mid-December (Figure 1c and Table 1). This indicates that positive net $bSiO_2$ production was light-limited during the latter stages of the autumn bloom and dissolution-dominated water column Si dynamics; while our incubations encouraged positive (net) production by alleviating light limitation.

Fundamental different mechanisms between blooms in spring (increasing stratification and irradiance) and autumn (declining stratification and irradiance; Figure 1b) may lead to differences in Si cycling. Spring diatom growth is encouraged by alleviation from light limitation and terminated by Si limitation as $Si(OH)_4$ is converted to $bSiO_2$ and exported, so (net) $bSiO_2$ production and export dominate Si-cycling. In contrast, our autumn observations imply that a large fraction of detrital $bSiO_2$, combined with suboptimal light conditions, limit net $bSiO_2$ production, with $bSiO_2$ dissolving, so that (net) $bSiO_2$ dissolution dominates.

In an ecosystem with a large $bSiO_2$ pool, the fraction of this pool that is living or detrital will determine whether continued production or dissolution dominates Si cycling. This balance between production or loss may also occur during the early stages of the spring bloom, as weak stratification establishes itself, but is eroded via mixing events until it overcomes these conditions (e.g., Daniels et al., 2015; Taylor & Ferrari, 2011). Attention should focus on determining the $bSiO_2$ pool composition and its growth dynamics in terms of living and detrital components to better understand surface ocean Si cycling.

Acknowledgments
We thank Phil Warwick for advice. We acknowledge support of the Captain, officers, and crew of DY018 cruise, as well as Jonathan Sharples (Chief Scientist). UK Natural Environmental Research Council (NERC) supported this study with grants NE/K001701/1 and NE/K002058/1. K. J. M. received a NERC Doctoral Training Partnership studentship (ref. 1498915). Data are held at the British Oceanographic Data Centre (http://www.bodc.ac.uk).

References

Barnett, M. L., Kemp, A. E. S., Hickman, A. E., & Purdie, D. A. (2019). Shelf sea subsurface chlorophyll maximum thin layers have a distinct phytoplankton community structure. *Continental Shelf Research*, *174*, 140–157. https://doi.org/10.1016/j.csr.2018.12.007

Beucher, C., Treguer, P., Corvaisier, R., Hapette, A. M., & Elskens, M. (2004). Production and dissolution of biosilica and changing microphytoplankton dominance in the Bay of Brest (France). *Marine Ecology Progress Series*, *267*, 57–69. https://doi.org/10.3354/meps267057

Beucher, C., Treguer, P., Corvaisier, R., Hapette, A. M., Pichon, J. J., & Metzl, N. (2004). Intense summer biosilica recycling in the Southern Ocean. *Geophysical Research Letters*, *31*, L09305. https://doi.org/10.1029/2003GL.018998

Bidle, K. D., & Azam, F. (1999). Accelerated dissolution of diatom silica by marine bacterial assemblages. *Nature*, *397*(6719), 508–512. https://doi.org/10.1038/17351

Bidle, K. D., & Azam, F. (2001). Bacterial control of silicon regeneration from diatom detritus; significance of bacterial ectohydrolases and species identity. *Limnology and Oceanography*, *46*(7), 1606–1623. https://doi.org/10.4319/lo.2001.46.7.1606

Bidle, K. D., Brzezinski, M. A., Long, R. A., Jones, J. L., & Azam, F. (2003). Diminished efficiency in the oceanic silica pump caused by bacteria-mediated silica dissolution. *Limnology and Oceanography*, *48*(5), 1855–1868. https://doi.org/10.4319/lo.2003.48.5.1855

Brown, L., Sanders, R., Savidge, G., & Lucas, C. H. (2003). The uptake of silica during the spring bloom in the Northeast Atlantic Ocean. *Limnology and Oceanography*, *48*(5), 1831–1845. https://doi.org/10.4319/lo.2003.48.5.1831

Brzezinski, M. A. (1985). The Si:C:N ratio of marine diatoms: Interspecific variability and the effect of some environmental variables. *Journal of Phycology*, *21*(1), 347–357. https://doi.org/10.1111/j.0022-3646.1985.00347.x

Brzezinski, M. A., Jones, J. L., Bidle, K. D., & Azam, F. (2003). The balance between silica production and silica dissolution in the sea: Insights from Monterey Bay, California, applies to the global data set. *Limnology and Oceanography*, *48*(5), 1846–1854. https://doi.org/10.4319/lo.2003.48.5.1846

Daniels, C. J., Poulton, A. J., Esposito, M., Paulsen, M. L., Bellerby, R., St. John, M., & Martin, A. P. (2015). Phytoplankton dynamics in contrasting early state North Atlantic spring blooms: Composition, succession and potential drivers. *Biogeosciences*, *12*(8), 2395–2409. https://doi.org/10.5194/bg-12-2395-2015

Dugdale, R. C., & Wilkerson, F. P. (1998). Silicate regulation of new production in the equatorial Pacific upwelling. *Nature*, *391*(6664), 270–273. https://doi.org/10.1038/34630

Field, C. B., Behrenfeld, M. J., Randerson, J. T., & Falkowski, P. (1998). Primary production of the biosphere: Integrating terrestrial and oceanic components. *Science*, *281*(5374), 237–240. https://doi.org/10.1126/science.281.5374.237

Findlay, H. S., Yool, A., Nodale, M., & Pitchford, J. W. (2006). Modelling of autumn plankton bloom dynamics. *Journal of Plankton Research*, *28*(2), 209–220. https://doi.org/10.1093/plankt/fbi114

Fragoso, G. M., Poulton, A. J., Yashayaev, I. M., Head, E. J. H., Johnsen, G., & Purdie, D. P. (2018). Diatom biogeography from the Labrador Sea revealed through a trait-based approach. *Frontiers in Marine Science*, *5*, 297. https://doi.org/10.3389/fmars.2018.00297

Green, J. A. M., Simpson, J. H., Legg, S., & Palmer, M. R. (2008). Internal waves, baroclinic energy fluxes and mixing at the European shelf edge. *Continental Shelf Research*, *28*(7), 937–950. https://doi.org/10.1016/j.csr.2008.01.014

Hamm, C. E., Merkel, R., Springer, O., Jurkojc, P., Maier, C., Prechtel, K., & Smetacek, V. (2003). Architecture and material properties of diatom shells provide effective mechanical protection. *Nature*, *421*(6925), 841–843. https://doi.org/10.1038/nature01416

Hickman, A. E., Holligan, P. M., Moore, C. M., Sharples, J., Krivtsov, V., & Palmer, M. R. (2009). Distribution and chromatic adaptation of phytoplankton within a shelf sea thermocline. *Limnology and Oceanography*, *54*(2), 525–536. https://doi.org/10.4319/lo.2009.54.2.0525

Hydes, D. J., Aoyama, M., Aminot, A., Bakker, K., Becker, S., Coverly, S., et al. (2010). Determination of dissolved nutrients (N, P, Si) in seawater with high precision and inter-comparability using gas-segmented continuous flow analysers, In: The GO-SHIP repeat hydrography manual: A collection of expert reports and guidelines. IOCCP report No. 14. ICPO publication series No. 134.https://archimer.ifremer.fr/doc/00020/13141/

Hydes, D. J., Le Gall, A. C., Miller, A. E. J., Brockmann, U., Raabe, T., Holley, S., et al. (2001). Supply and demand of nutrients and dissolved organic matter at and across the NW European shelf break in relation to hydrography and biogeochemical activity. *Deep Sea Research, Part II*, *48*(14-15), 3023–3047. https://doi.org/10.1016/S0967-0645(01)00031-5

Krause, J. W., Nelson, D. M., & Lomas, M. W. (2010). Production, dissolution, accumulation, and potential export of biogenic silica in a Sargasso Sea mode-water eddy. *Limnology and Oceanography*, *55*(2), 569–579. https://doi.org/10.4319/lo.2010.55.2.0569

Lindeman, C., & St. John, M. A. (2014). A seasonal diary of phytoplankton in the North Atlantic. *Frontiers in Marine Science*, *1*, 37. https://doi.org/10.3389/fmars.2014.00037

Martin-Jezequel, V., Hildedrand, M., & Brezinski, M. A. (2000). Silicon metabolism in diatoms: implications for growth. *Journal of Phycology*, *36*(5), 821–840. https://doi.org/10.1046/j.1529-8817.2000.00019.x

Natori, Y., Haneda, A., & Suzuki, Y. (2006). Vertical and seasonal differences in biogenic silica dissolution in natural seawater in Suruga Bay, Japan: Effects of temperature and organic matter. *Marine Chemistry*, *102*(3-4), 230–241. https://doi.org/10.1016/j.marchem.2006.04.007

Nelson, D. M., DeMaster, D. J., Dunbar, R. B., & Smith, W. O. Jr. (1996). Cycling of organic carbon and biogenic silica in the Southern Ocean: Estimates of water-column and sedimentary fluxes on the Ross Sea continental shelf. *Journal of Geophysical Research*, *101*(C8), 18,519–18,532. https://doi.org/10.1029/96JC01573

Nelson, D. M., Tréguer, P., Brzezinski, M. A., Leynaert, A., & Quéguiner, B. (1995). Production and dissolution of biogenic silica in the ocean: Revised global estimates, comparison with regional data and relationship to biogenic sedimentation. *Global Biogeochemical Cycles*, *9*(3), 359–372. https://doi.org/10.1029/95GB01070

Painter, S. C., Finlay, M., Hemsley, V. S., & Martin, A. P. (2016). Seasonality, phytoplankton succession and the biogeochemical impacts of an autumn storm in the northwest Atlantic Ocean. *Progress in Oceanography*, *142*, 72–104. https://doi.org/10.1016/j.pocean.2016.02.001

Perry, M. J., Sackman, M. S., Eriksen, C. C., & Lee, C. M. (2008). Seaglider observations of blooms and subsurface chlorophyll maxima off the Washington coast. *Limnology and Oceanography*, *53*(5part2), 2169–2179. https://doi.org/10.4319/lo.2008.53.5_part_2.2169

Poulton, A. dissolved nutrients (N,J., Davis, C. E., Daniels, C. J., Mayers, K. M. J., Harris, C., Tarran, G. A., et al. (2018). Seasonal phosphorus and carbon dynamics in a temperate shelf sea (Celtic Sea). *Progress in Oceanography*. https://doi.org/10.1016/j.pocean.2017.11.001

Poulton, A. J., Sanders, R., Holligan, P. M., Stinchcombe, M. C., Adey, T. R., Brown, L., & Chamberlain, K. (2006). Phytoplankton mineralization in the tropical and subtropical Atlantic Ocean. *Global Biogeochemical Cycles*, *20*, GB4002. https://doi.org/10.1029/2006GB002712

Ragueaneau, O., & Tréguer, P. (1994). Determination of biogenic silica in coastal waters: applicability and limits of the alkaline digestion method. *Marine Chemistry*, *45*(1-2), 43–51. https://doi.org/10.1016/0304-4203(94)90090-6

Ruiz-Castillo, E., Sharples, J., Hopkins, J., & Woodward, E. M. S. (2018). Seasonality in the cross-shelf physical structure of a temperate shelf sea and the implications for nitrate supply. *Progress in Oceanography* . https://doi.org/10.1016/j.pocean.2018.07.006

Sharples, J., Moore, C. M., Hickman, A. E., Holligan, P. M., Tweddle, J. F., Palmer, M. R., & Simpson, J. H. (2009). Internal tidal mixing as a control on continental margin ecosystems. *Geophysical Research Letters*, *36*, L23603. https://doi.org/10.1029/2009GL040683

Taylor, J. R., & Ferrari, R. (2011). Shutdown of turbulent convection as a new criterion for the onset of spring phytoplankton blooms. *Limnology and Oceanography*, *56*(6), 2293–2307. https://doi.org/10.4319/lo.2011.56.6.2293

Tréguer, P. J., Bowler, C., Moriceau, B., Dutkiewicz, S., Gehlen, M., Aumont, O., et al. (2018). Influence of diatom diversity on the ocean biological carbon pump. *Nature Geoscience*, *11*(1), 27–37. https://doi.org/10.1038/s41561-017-0028-x

Tréguer, P. J., & De La Rocha, C. L. (2013). The world ocean silica cycle. *Annual Review of Marine Science*, *5*(1), 477–501. https://doi.org/10.1146/annurev-marine-121211-172346

Tréguer, P., Nelson, D. M., Van Bennekom, A. J., Demaster, D. J., Leynaert, A., & Quéguiner, B. (1995). The balance of silica in the world ocean: A re-estimate. *Science*, *268*, 375–379. https://doi.org/10.1126/science.268.5209.375

Van Cappellen, P., Dixit, S., & van Beusekom, J. (2002). Biogenic silica dissolution in the oceans: reconciling experimental and field-based dissolution rates. *Global Biogeochemical Cycles*, *16*(4), 1075. https://doi.org/10.1029/2001GB001431

Vlasenko, V., Stashcuk, N., Inall, M. E., & Hopkins, J. E. (2014). Tidal energy conversion in a global hot spot: One the 3-D dynamics of baroclinic tides at the Celtic Sea shelf break. *Journal of Geophysical Research: Oceans*, *119*, 3249–3265. http://doi.org/10.1002/2013JC009708

Widdicombe, C. E., Eloire, D., Harbour, D., Harris, R. P., & Somerfield, P. J. (2010). Long-term phytoplankton community dynamics in the Western English Channel. *Journal of Plankton Research*, *32*(5), 643–655. https://doi.org/10.1093/plankt/fbp127

Wihsgott, J. U. (2018). A tale of four seasons: Investigating the seasonality of physical structure and its biogeochemical response in a temperate continental shelf sea. PhD thesis, University of Liverpool.

Wihsgott, J. U., Hopkins, J. E., Sharples, J., Jones, E., & Balfour, C. (2016). Long-term mooring observations of full depth water column structure spanning 17 months, collected in a temperate shelf sea (Celtic sea) on the NW European Shelf. *British Oceanographic Data Centre.*. https://doi.org/10.5285/389fe406-ebd9-74f1-e053-6c86abc032a4

Wihsgott, J. U., Hopkins, J. E., Sharples, J., Jones, E., & Balfour, C. (2018). Long-term, full depth observations of horizontal velocities spanning 17 months, collected in a temperate shelf sea (Celtic sea) on the NW European Shelf. British Oceanographic Data Centre. https://doi.org/10.5285/631ddd2a-48df-143b-e053-6c86abc0d49f.

Wihsgott, J. U., Sharples, J., Hopkins, J. E., Woodward, E. M. S., Hull, T., Greenwood, N., & Sivyer, D. B. (2019). Observations of vertical mixing in autumn and its effect on the autumn phytoplankton bloom. *Progress in Oceanography*. https://doi.org/10.1016/j.pocean.2019.01.001

Woodward, E. M. S., & Rees, A. P. (2001). Nutrient distributions in an anti-cyclonic eddy in the North East Atlantic Ocean, with reference to nano-molar ammonium concentrations. *Deep Sea Research, Part II*, *48*(4-5), 775–793. https://doi.org/10.1016/S0967-0645(00)00097-7